Double Heterojunction Laser Diode (Tucker Model) DHLD

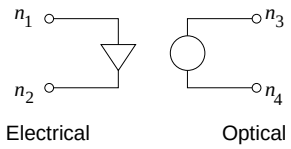

Figure 1: DHLD — Double Heterojunction Laser Diode (Tucker model).

fREEDA Form: DHLD:⟨instance name⟩ n_1 n_2 n_3 n_3 ⟨parameter list⟩

n_1 is the electrical anode terminal

n_2 is the electrical cathode or reference electrical

n_3 is the optical terminal

n_3 is the optical reference terminal

parameter list see table for parameter list

Parameter Table

Parameters	Description	Values	Units
R_s	series resistance	2	Ω
R_e	equivalent resistance due to carrier degeneracy	0.468	Ω
I_{01}	equivalent Diode1 leakage current	2.54e-25	A
I_{02}	equivalent Diode2 leakage current	18.13e-3	A
b	current controlled current source gain	6.92	A^{-1}
τ_{ns}	equivalent recombination Lifetime	2.25e-9	s
C_0	diode zero-bias charge capacitance	10e-12	F
V_D	junction built-in potential	1.65	V
D	constant relating the radiative recombination current per unit volume to the optical gain	1.79e-29	$V^{-1}A^{-1}m^6$
a	fraction of equivalent recombination lifetime over low-level injection spontaneous recombination lifetime	0.125	-
R_p	equivalent optical resistor	29.4	Ω
C_p	equivalent optical capacitor	0.102e-12	F
S_c	photon density normalization constant	1e21	m^{-3}
β	fraction of spontaneous emission coupled into the lasing mode	1e-3	-

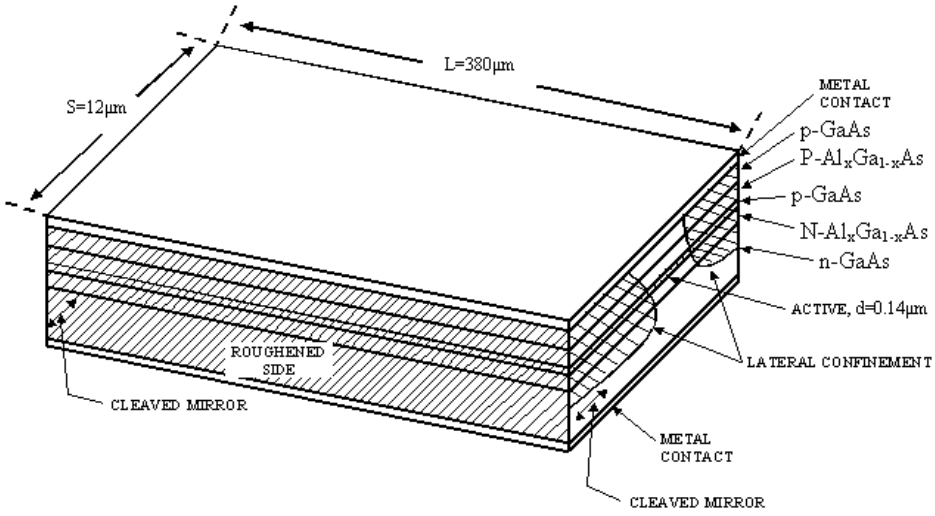

Figure 2: Double-heterostructure laser. The *p-GaAs* active layer is usually less than 0.5 μm thick. After [14, 15].

The DHLD consists of a p-type GaAs active layer of thickness d sandwiched between n-type and p-type layers of higher bangap material as shown in Fig. 2. The circuit model for the DHLD is shown in Fig. 3. It is similar in many ways to the structure described in [11]. The laser diode model is based on the Tucker large-signal circuit model [12, 13]. It is derived from the physics of the heterojunction and explicitly takes into account the effect of carrier degeneracy, high level injection, and nonradiative recombination. The modulation response is determined through the rate equations of the device's electro-optical dynamics. The model is described in Chapter 3 of Reference [1].

Analysis

Under the assumption that the thickness d of the active layer is small compared to the carrier diffusion length and that the variation of carrier densities with position in the active layer is small enough [12], the carrier densities can be represented by average values. Then the average total electron density N in the active layer is given by

$$N = N_0 + n \tag{1}$$

where N_0 is the equilibrium electron density and n is the excess electron density. Corresponding notation can be used for hole densities.

From the physics of the Heterostructure1 lasers [11, 12], and under the above assumptions, the total radiative spontaneous recombination rate R in the active layer is given by:

$$R = BNP \tag{2}$$

where B is a constant and P is the average total hole density in the active layer [12]. To obtain the diode current due to spontaneous radiative recombination, we define the excess spontaneous radiative recombination rate r_e as:

$$r_e = n/\tau_s + B_1 n^2 \tag{3}$$

where τ_s is the low-level injection spontaneous recombination lifetime and B_1 is a constant defined in [12].

Also, a significant contribution to the diode current arises from nonradiative recombination rate r_n along the strip edges and at the heterointerfaces. Following the analysis in [11], it is assumed here that the nonradiative recombination rate is proportional to n, and is characterized by a lifetime τ_n. Then the total excess recombination rate r_t (including radiative and nonradiative components) is obtained by adding the

nonradiative recombination rate $r_n = n/\tau_n$ to r_e:

$$r_t = (1/\tau_n + 1/\tau_s)n + B_1 n^2 \ . \tag{4}$$

Again, since the active layer is assumed to be thin, the diode recombination current is obtained by multiplying r_t by the active layer volume v_a and the electron charge q. Adding to it the displacement-current term, we obtain the diode terminal current below threshold I:

$$I = qv_a \left(r_t + \frac{dn}{dt} \right) \ . \tag{5}$$

Note that Eqn. 5 does not include the effects of space-charge capacitance. Substituting Eqn. 4 in Eqn. 5 gives:

$$I = I_1 + bI_1^2 + \tau_{ns} \frac{dI_1}{dt} \tag{6}$$

where

$$I_1 = \frac{qv_a n}{\tau_{ns}} \tag{7}$$

$$b = \frac{B_1 \tau_{ns}^2}{qv_a} \tag{8}$$

and

$$\tau_{ns} = (\tau_s^{-1} + \tau_n^{-1})^{-1} \tag{9}$$

Current/Voltage characteristics
The diode junction voltage V_j can be expressed in terms of the electron density in the active layer as a three series-connected voltage drops V_1, V_2, and V_3. That is:

$$V_j = V_1 + V_2 + V_3 \tag{10}$$

and

$$V_1 = V_T \ln(1 + n/N_0) \tag{11}$$

$$V_2 = V_T \ln\{1 + n/(N_A + N_0)\} \tag{12}$$

$$V_3 = V_T(\alpha_1 + \alpha_3)n \tag{13}$$

where $V_T = kT/q$ is the thermal voltage, N_A is the acceptor impurity concentration, and α_1 and α_2 are constant defined in [12]. The first two of these elements represent a classical Shockley p-n junction diodes. With Eqn. 7 substituted, Eqns. 11 and 12 become:

$$I_1 = I_{01}\{\exp(V_1/V_T) - 1\} \tag{14}$$

and

$$I_1 = I_{02}\{\exp(V_2/V_T) - 1\} \tag{15}$$

where I_1 is the current through the two diodes and the two diode leakage currents are given by:

$$I_{01} = qv_a N_0/\tau_{ns} \tag{16}$$

and

$$I_{02} = qv_a(N_A + N_0)/\tau_{ns} \tag{17}$$

The third series-connected element is given by Eqn. 13. Substituting Eqn. 7 in Eqn. 13 gives

$$I_1 = V_3/R_e \tag{18}$$

where

$$R_e = (\alpha_1 + \alpha_3) N_0 V_T / I_{01} \ . \tag{19}$$

Rate Equations

As mentioned earlier, the excess spontaneous recombination rate per unit volume r_t can be written as the sum of two components r_n and r_e:

$$r_t = r_n + r_e \tag{20}$$

Then, the total diode current due to spontaneous recombination is $I_t = q v_a r_t$, which can be written in the form:

$$I_t = I_1 + b I_1^2 \tag{21}$$

and the diode current due to radiative spontaneous recombination is $I_e = q v_a r_e$, which reduces to:

$$I_e = a I_1 + b I_1^2 \tag{22}$$

where

$$a = \tau_{ns} / \tau_s \tag{23}$$

The single mode rate equations for an injection laser [13] can be written in the form

$$q v_a \frac{dn}{dt} = I - I_t - q v_a g S \tag{24}$$

$$q v_a \frac{dS}{dt} = q v_a g S - \frac{S q v_a}{\tau_p} + \beta I_e \tag{25}$$

where I is the diode terminal current, g is the optical gain, S is the photon density in the active layer, τ_p is the photon lifetime, and β is the fraction of spontaneous emission coupled into the lasing mode. Eqn. 24 describes electron-injection and charge-storage effects in the active layer, and Eqn. 25 describes the corresponding injection and storage dynamics of photons. These equations form the basis of the equivalent large signal model. To account for the space-charge storage in the heterojunction layer, Eqn. 24 is generalized to include space-charge capacitance term. Note that this effect is taken into account by a capacitor C_s and is different from the charge-storage effect taken into account by the term $\tau_{ns} dI_1/dt$. Also, a normalized photon density S_n is introduced to obtain better numerical values. With the above modifications, and substituting Eqns. 21 and 22, the rate equations become:

$$I = I_1 + b I_1^2 + \tau_{ns} \frac{dI_1}{dt} + C_s \frac{dVj}{dt} + G S_n \tag{26}$$

$$G S_n + \beta (a I_1 + b I_1^2) = \frac{S_n}{R_p} + C_p \frac{dS_n}{dt} \tag{27}$$

where $C_s = C_0 (1 - V_j / V_D)^{-1/2}$ is the space-charge capacitance, V_J is the heterojunction voltage, C_0 is the zero bias space-charge capacitance, V_D is the diode built-in potential, $C_P = q v_a S_c$, $G = g C_p$, $R_p = \tau_p / C_p$, and $S_n = S / S_c$, where S_c is the photon-density normalization constant.

Equivalent Large-signal Circuit Model

The large-signal circuit model of the injection laser follows from the rate equations, Eqns. 26 and 27, and from the current/voltage characteristics of the diode. The electrical equivalent model is shown to the left of the vertical broken line in Fig. 3. It is important to note that the resistance R_e in series with the two Shockley diodes arises from carrier degeneracy, and is not associated with the ohmic regions of the diode. Those regions are modelled by a series resistance R_s which includes contributions from lead resistance, bulk resistance in the high-bandgap materials, and the effective resistance of the near-ohmic p-P isotype

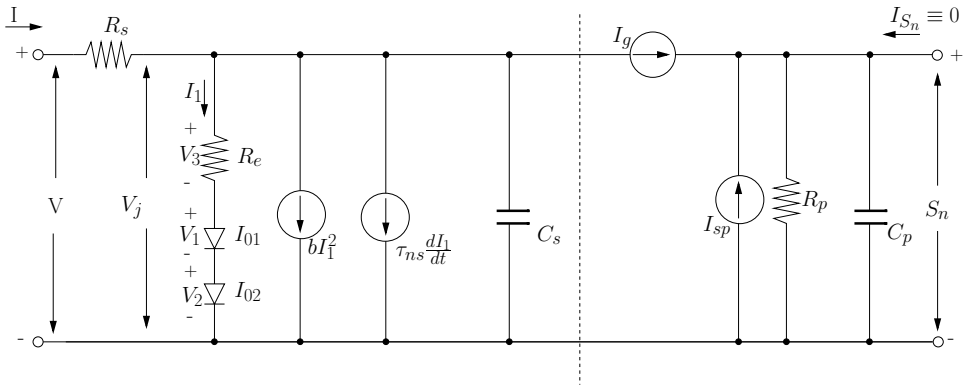

Figure 3: Large-signal two port circuit model of injection laser

heterojunction. The resulting equivalent circuit model of the photon dynamics is shown to the right of the vertical broken line in Fig. 3 and is derived from Eqn. 27. where

$$I_{sp} = \beta(aI_1^2 + bI_1^2) \tag{28}$$

and

$$I_g = GS_n \ . \tag{29}$$

Diode Parameters

The laser parameters used in the simulations are the same as the ones used in [12, 13], and are similar to the parameters used in [11]. The excess electron density in the active layer is assumed to be $n_s = 1.5\times10^{18}$ cm^{-3}, and the factor qv_a is taken as 1.02×10^{-25} mA cm^3 s. Thus the threshold current I_t is approximately 100 mA. The active layer doping density is taken as $N_A = 4 \times 10^{17}$ cm^{-3}, and the photon lifetime is $\tau_p = 3.0$ ps.

It is also assumed that the optical gain function G has a square-law dependence on the radiative recombination current per unit volume J_{nom} as described in [14]

$$G = D(J_{nom} - 2 \times 10^{13})^2 \tag{30}$$

where D is a constant and $J_{nom} = I_e/v_a$ A/m^3.A numerical value of D can be obtained by first determining S_{n0}, the steady-state normalized photon density, and then setting it to infinity at saturation, that is when $n = n_s$. The steady-state photon density is obtained by subsrituting $dS_n/dt = 0$ in Eqn. 27

$$S_{n0} = \frac{\beta(aI_{10} + bI_{10}^2)}{1/R_p - G} \tag{31}$$

where I_{10} is the steady-state value of I_1. As we can see, S_{n0} goes to infinity when $G = 1/R_p$ which, when substituted in Eqn. 30, yields

$$D = R_p^{-1}(J_{noms} - 2 \times 10^{13})^{-2} \tag{32}$$

where J_{noms} is the value of J_{nom} at saturation, and is given by

$$J_{noms} = \frac{qn_s}{\tau_{ns}}(a + b\frac{qv_a n_s}{\tau_{ns}}) \tag{33}$$

with the known diode parameters substituted in Eqns. 33 and 30, we obtain $J_{noms} = 6.359 \times 10^{13}$ and $D = 1.79 \times 10^{-29}$ V^{-1} A^{-1} m^6. Numerical values of other parameters of the circuit model are listed in Table **??**.

Implementation

The key to the implementation of the model is to consider the voltage on one of the diodes in Fig. 3 as the first state variable, V_1 for example, and the normalized photon density S_n as the second state variable, and then write the model equations as a function of these two state variables and there derivatives, *i.e.* dV_1/dt and dS_n/dt .

The relation between the drive input voltage V and current I is given by:

$$V = IR_s + V_j \tag{34}$$

where I can be expressed as:

$$I = I_1 + bI_1^2 + \tau_{ns}\frac{dI_1}{dt} + C_s\frac{dV_j}{dt} + I_g \tag{35}$$

To write Eqns. 34 and 35 in terms of the state variables and there derivatives, we need to find I_1, dI_1/dt, V_j, and dV_j/dt in terms of these state variables. From Eqn. 14, we know that $I_1 = I_{01}\{\exp(V_1/V_T) - 1\}$, then

$$\frac{dI_1}{dt} = \frac{I_{01}}{V_T}\exp(V_1/V_T)\frac{dV_1}{dt} \tag{36}$$

and V_j can be expressed as:

$$V_j = V_1 + V_2 + V_3 \tag{37}$$

where

$$V_2 = V_T ln(I_1/I_{02} + 1) \tag{38}$$

and

$$V_3 = I_1 R_e \cdot \tag{39}$$

We still have to write dV_j/dt as a function of the state variables and their derivatives:

$$\frac{dV_j}{dt} = \frac{dV_1}{dt} + \frac{dV_2}{dt} + \frac{dV_3}{dt} \tag{40}$$

where from Eqn. 38, we have

$$\frac{dV_2}{dt} = \frac{I_{01}}{I_{02}}\exp\{\frac{(V_1 - V_2)}{V_T}\}\frac{dV_1}{dt} \tag{41}$$

and from Eqn. 39, we have

$$\frac{dV_3}{dt} = R_e\frac{dI_1}{dt} \ . \tag{42}$$

Finally, we have to find I_g as a function of the state variables. We know that $I_g = GS_n = D(J_{nom} - 2 \times 10^{13})^2 S_n$, and that $J_{nom} = I_e/v_a = (aI_1 + bI_1^2)/v_a$, then

$$I_g = D(\frac{aI_1 + bI_1^2}{v_a} - 2 \times 10^{13})^2 S_n \ . \tag{43}$$

Now that we have expressed the current I and voltage V at the electrical port of the diode as a function of the state variables, we have to express the current and voltage at the optical port of the diode as a function of those variables. The voltage at the optical port is chosen to be S_n, however, the current I_{sn} has no meaning and it is forced to be zero ($I_{sn} \equiv 0$) by connecting an open circuit to the optical port. The model, however, will not function properly unless the Eqn. 27 is satisfied. This is done by using the fact that $I_{sn} \equiv 0$ and by rewriting Eqn. 27 in the form[1]

$$I_{sn} = GS_n + \beta(aI_1 + bI_1^2) - \frac{S_n}{R_p} - C_p\frac{dS_n}{dt} \tag{44}$$

[1]Another way to satisfy Eqn. 27 is to connect a 1 Ω resistor at the optical port and make use of the fact that $I_{sn} - S_n \equiv 0$, where $I_{sn} = R_pGS_n + R_p\beta(aI_1 + bI_1^2) - R_pC_p\frac{dS_n}{dt}$. This implementation actually will not result in a singular matrix in Harmonic-balance simulations and alleviate the need to use a large resistance instead of the open circuit in that case.

One last thing we did not talk about above is parameterization or variable transformations. They both refer to an algebraic transformation of the device equations that leads to a better convergence properties, and enables universal device modeling. The parameterization employed here is the one suggested in [16] and that converts the strong nonlinear current-voltage relationship of the diode to two smoother functions of current and voltage as functions of the state-variable x. Specifically, V_1 is not taken as the state variable in the actual coding, and Eqn. 14 is parameterized as follows

$$I_1 = \begin{cases} I_{01}\{\exp(\alpha x) - 1\} & \text{if } x \leq V_{pr} \\ I_{01}\exp(\alpha V_{pr})\{1 + \alpha(x - V_{pr})\} - I_{01} & \text{if } x > V_{pr} \end{cases} \tag{45}$$

$$V_1 = \begin{cases} x & \text{if } x \leq V_{pr} \\ V_{pr} + \frac{1}{\alpha}\ln\{1 + \alpha(x - V_{pr})\} & \text{if } x > V_{pr} \end{cases} \tag{46}$$

where $\alpha = 1/V_T$ and V_{pr} plays the role of a free parameter chosen appropriately to optimize the performance of the HB algorithm specifically. Experience shows [16] that $V_{pr} = \ln(1/\alpha I_s)/\alpha$ results in excellent behavior of the model in most practical situations. As shown in Fig. 4, 5, and 6, the strong nonlinearity between i & v is converted to moderate nonlinearities between i & x and v & x, and the problem becomes well behaved. Please refer to [10] and [17] for more information on universal device modeling, and how the same piece of code is used in fREEDA with different simulation algorithms, *i.e.* HB, Transient, DC analysis, etc.

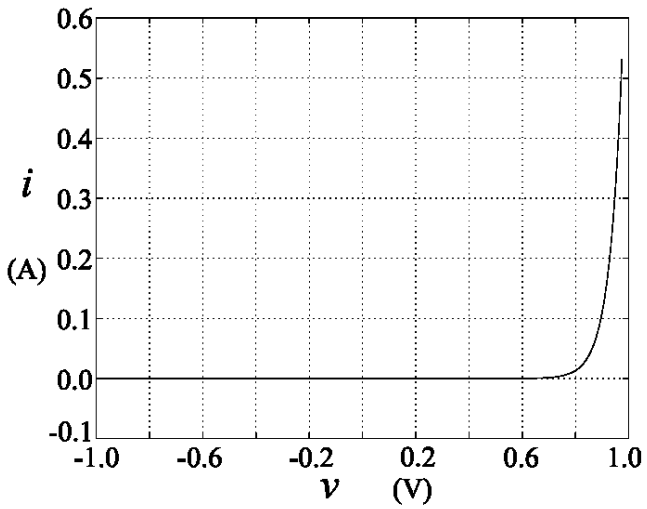

Figure 4: Relation between v and i in a diode.

Results

The following sections present the simulation results of the DHLD model. The diode is driven by an input current pulse of finite rise and fall time. Graphs of the input terminal voltage and of the normalized photon density are shown for different values of β and compared with HSPICE®.

A Harmonic Balance analysis is performed on the implemented DHLD model. First, the model is driven by a DC bias source and single tone sine wave. Plots of the input terminal voltage and of the normalized photon density are shown and compared with fREEDA's transient analysis and HSPICE®. Second, the model is driven by a DC bias source and two tone input sine waves. Plots of the optical output power spectrum is presented. Also, the power ratio of the second harmonic to the fundamental P_{2f}/P_f and of the intermodulation distortion to the fundamental P_{IM3}/P_f as a function of bias current are shown.

Transient Analysis

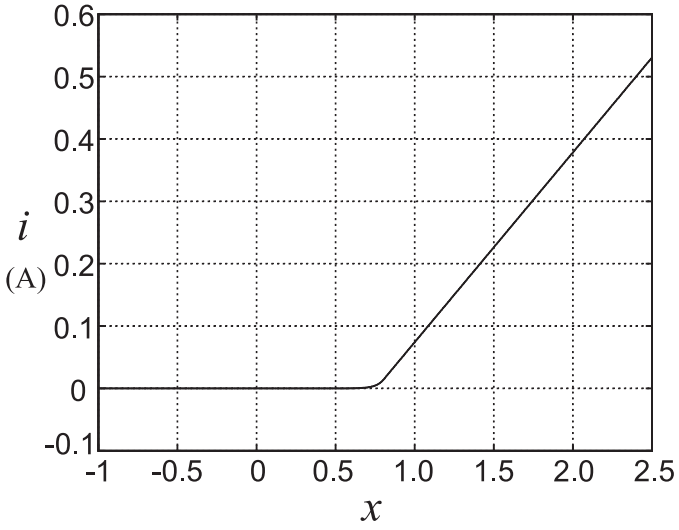

Figure 5: Relation between x and i in a diode.

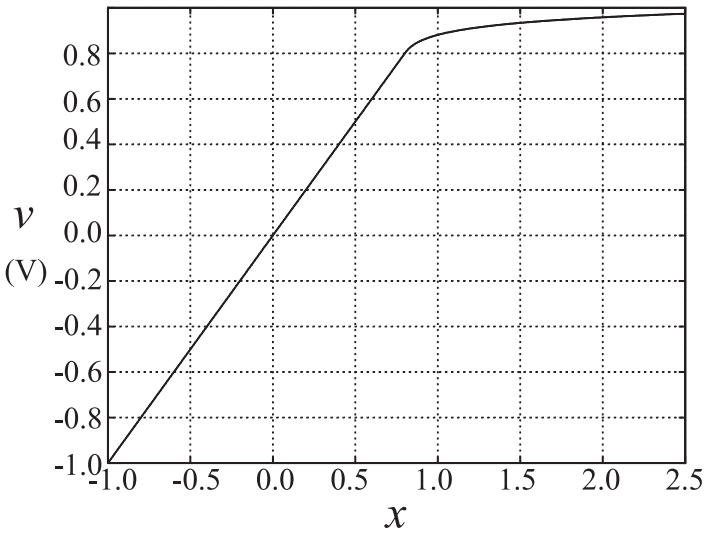

Figure 6: Relation between x and v in a diode.

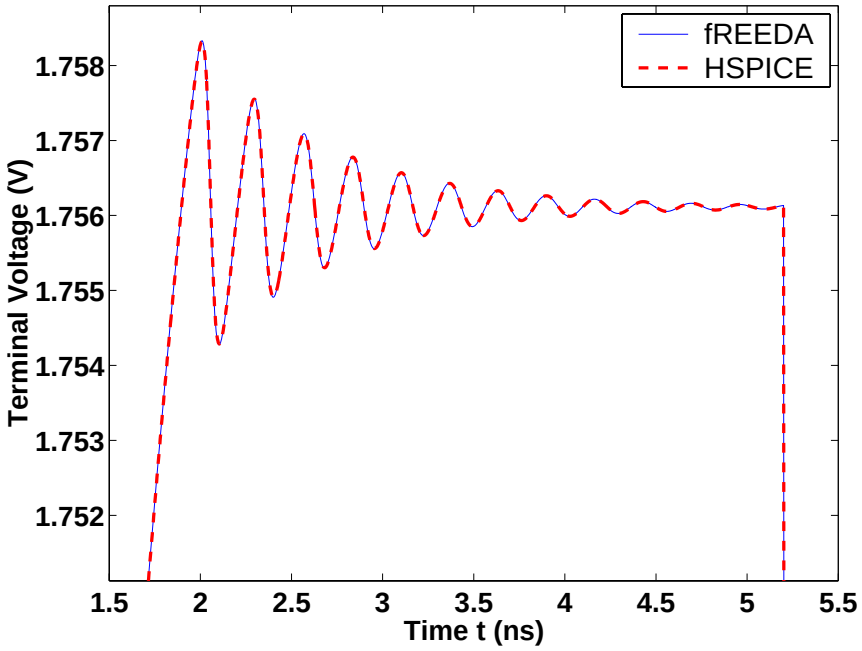

Figure 7: Transient analysis comparison of the terminal voltage

In the analysis and design of laser diode transmitter, it is very important to determine laser turn-on delay and other switching and modulation characteristics especially for high-speed application where the switching waveform is affect by the finite bandwidth of the drive circuits [12]. This is why transient simulation is very important in the design of optoelectronic ICs.

The DHLD model is driven by a current pulse that has a peak value of 150 mA and a rise time of 0.1 ns and the simulations are presented for different values of β. The plots in Fig. 7 shows the input terminal voltage versus time while the plots in Fig. 8 shows the normalized output photon density. As we can see, a very small change in the input voltage correspond to a large ringing effect in the output power and this is due to exponential current/voltage relationship of the diode. Also, Fig. 8 shows the laser turn-on delay.

As shown in all of the plots, there is excellent agreement between fREEDA and HSPICE®.

Harmonic Balance

Fiber-optic microwave links have the potential to be used in a large number of applications such as cable television systems and personal communication systems. That is why it is important to characterize the behavior of the laser diode under direct microwave intensity modulation, and one of the most important tools in the simulations of nonlinear models at microwave frequencies is Harmonic Balance.

The laser diode was connected to the parasitics and matching network as shown in Fig. 9 and harmonic balance simulations with a single and two tone sine wave input were performed.

The intensity modulation response of a double heterojunction laser diode to an rf-input input power of 7 dBm at 1 GHz at a bias current of 125 mA was simulated. The time domain results are shown in Figs. 10 and 11 and compared to transient analysis. The calculated optical output power spectrum is shown in Fig. 12, with the second harmonic being approximately 7.59 dBc.

Fig. 13 shows the power ratio of the second harmonic to the fundamental P_{2f}/P_f as a function of the bias current for an rf-input input power of 3 dBm at input frequency of 1 GHz. The threshold current of this device is 100 mA.

Finally, Fig. 14 shows the power ratio of the third-order intermodulation products to the carrier P_{IM3}/P_f

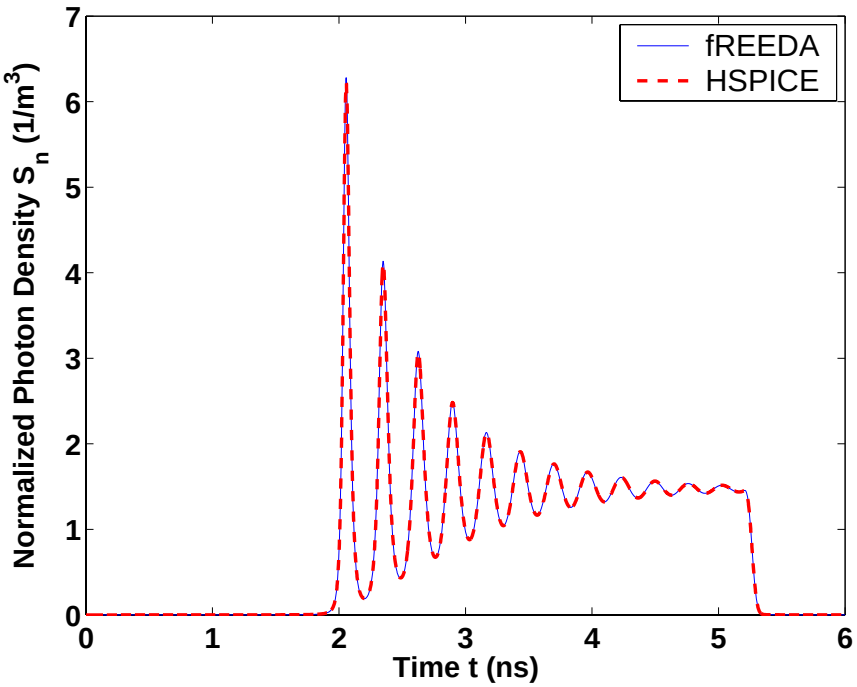

Figure 8: Transient Analysis comparison of the light output

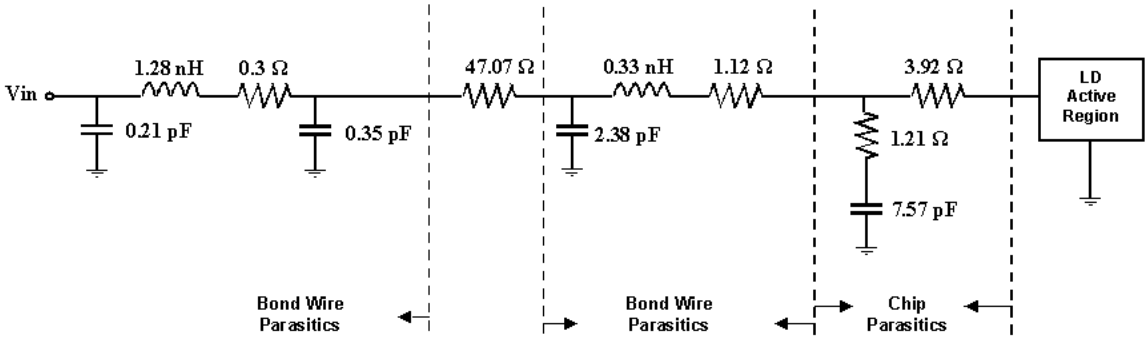

Figure 9: Parasitics and matching network used in HB simulation. After [18].

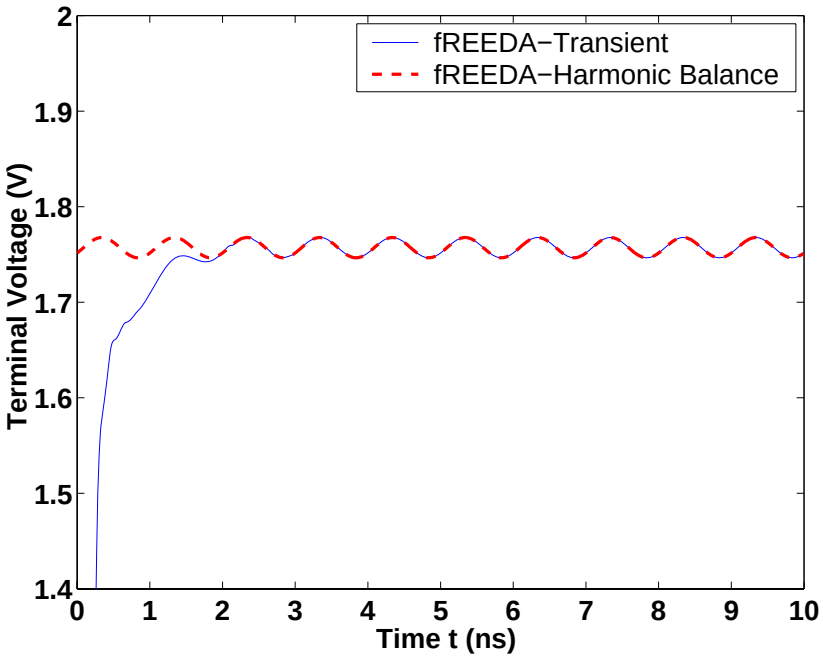

Figure 10: Comparison of the input terminal voltage between HB analysis and transient analysis in fREEDA.

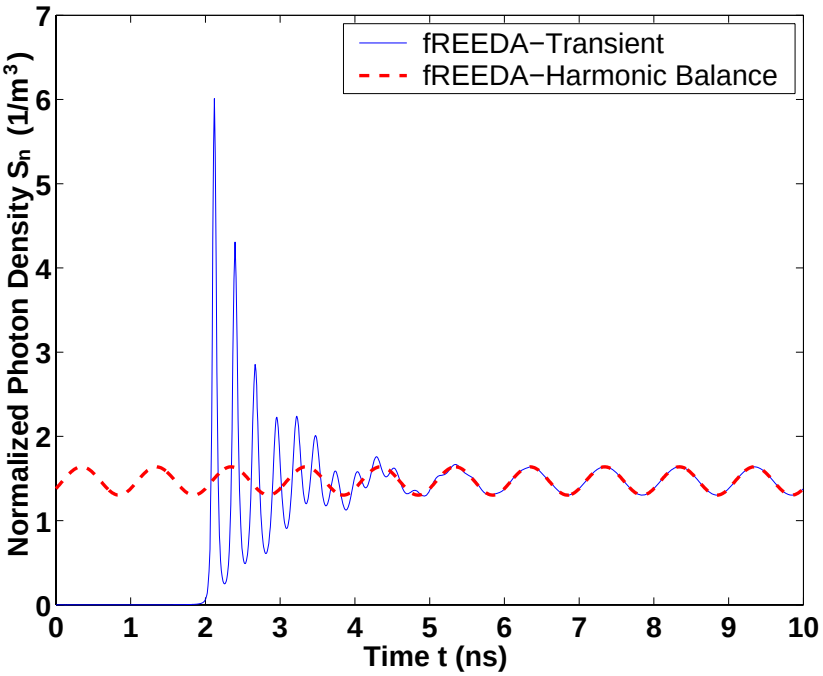

Figure 11: Comparison of the output photon density between HB analysis and transient analysis in fREEDA.

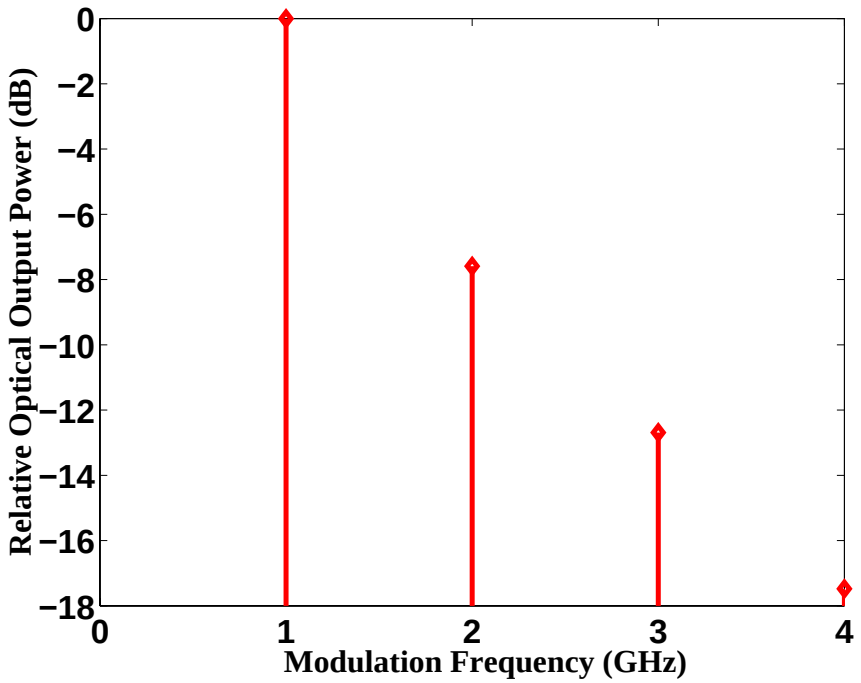

Figure 12: Large-signal intensity modulation response.

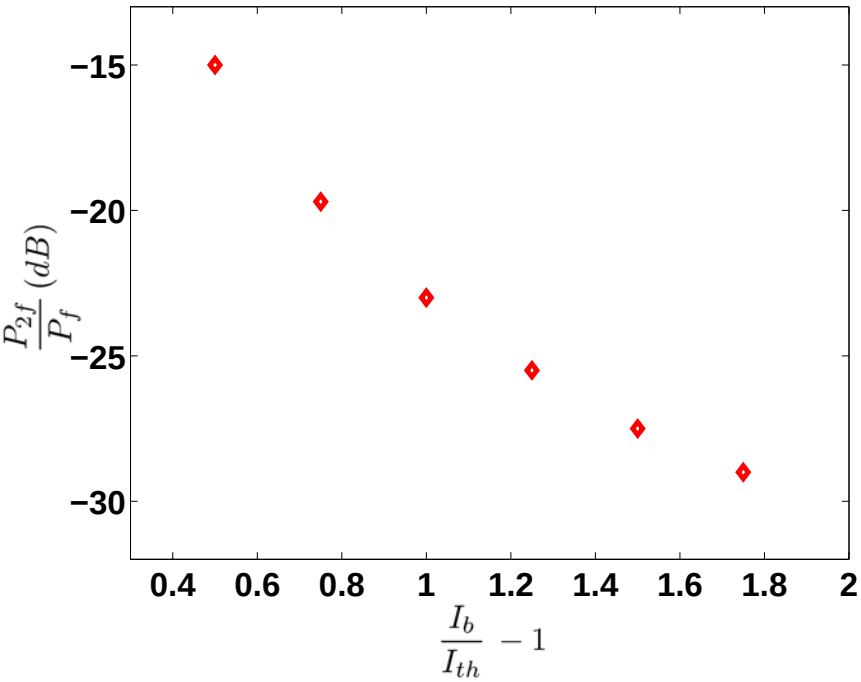

Figure 13: Power ratio of second harmonic to fundamental as a function of bias current.

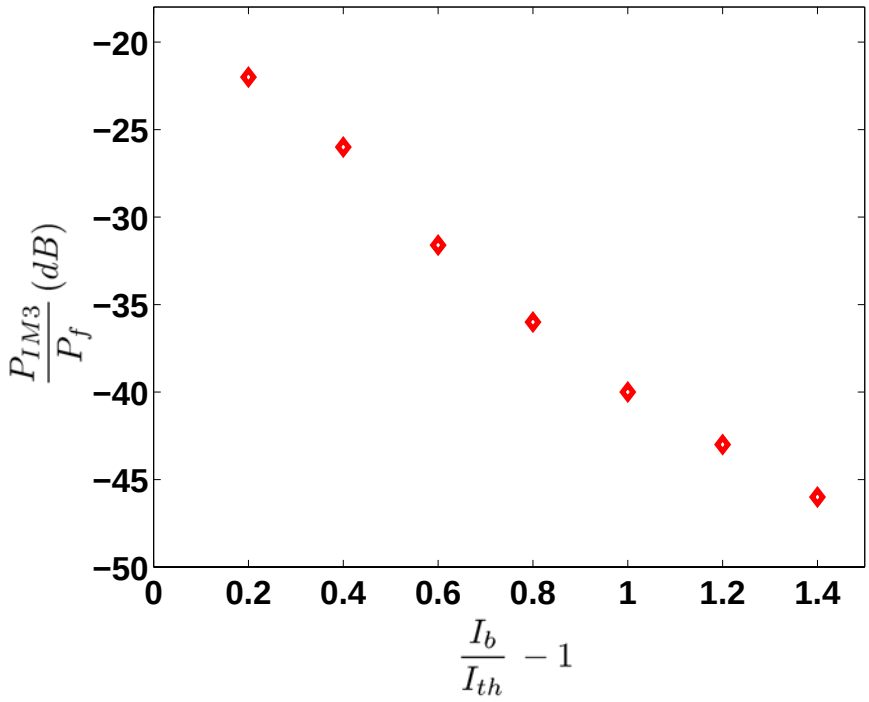

Figure 14: Power ratio of third-order intermodulation products to carrier as a function of bias current.

as a function of the bias current. Equal inputs of -1 dBm at 1.0 GHz and 1.04 GHz were used. In general, there is an improvement in linearity with increasing bias current.

As we can see, there is an excellent agreement in the single tone simulations between HB and transient analysis except at the beginning with HB which truncates the transient response. In addition, the two tone simulations shows a close agreement with the reported nonlinear distortion simulations in the literature [18, 19].

References

[1] H. Kanj, Circuit-Level Modeling of Laser Diodes , M.S., North Carolina State University, 2003

[2] N. Bewtra, D. A. Suda, G. L. Tan, F. Chatenoud, and J. M. Xu, "Modeling of Quantum-Well Lasers with Electro-Opto-Thermal Interaction," *IEEE J. of Selected Topics in Quantum Electronics*, Vol. 1, No. 2, pp. 331-340, June 1995.

[3] J. Morikuni, G. Dare, P. Mena, A. Harton, K. Wyatt, "Simulation of optical interconnect devices, circuits, and systems using analog behavioral modeling tools," *IEEE Lasers and Electro-Optics Society Annual Meeting*, Vol. 1, pp. 235–236, Dec 1998.

[4] *http://www.freeda.org.*

[5] A. Griewank, D. Juedes and J. Utke, "Adol-C: A Package for the Automatic Differenciation of Algorithms Written in C/C++" ACM TOMS, Vol. 22(2), pp. 131-167, June 1996.

[6] J. Hecht, "Laser Pioneers" *Boston: Academic Press*, 1992.

[7] R. D. Dupuis "An Introduction to the Developement of the Semiconductor Laser" *IEEE J. of Quantum Electronics*, Vol. QE-23, No. 6, June 1987.

[8] J. Morikuni, P. Mena, A. Harton, K. Wyatt, "Optoelectronic Computer-Aided Design," *IEEE Lasers and Electro-Optics Society Summer Topical Meetings*, pp. 53–54, July 1998.

[9] L. Seung-Woo, C. Eun-Chang, C. Woo-Young, "Optical interconnection system analysis using SPICE, " *The Pacific Rim Conference on Lasers and Electro-Optics*, Vol. 2, pp. 391–392, Sep 1999.

[10] C. E. Christoffersen, *Global Modeling of Nonlinear Microwave Circuits*, Ph.D. Dissertation, Dept. of Electrical Engineering, North Carolina State University, 2001.

[11] W. B. Joyce, R. W. Dixon, "Electrical characterization of heterostructure lasers," *in J. Appl. Phys.*, Vol. 49, No. 7, July 1978.

[12] R. S. Tucker, "Circuit model of double-heterojunction laser below threshold," *in IEE Proc. on Solid-State & Electron Devices–Part I*, Vol. 128, No. 3, pp. 101–106, 1981.

[13] R. S. Tucker, "Large-signal circuit model for simulation of injection-laser modulation dynamics," *in IEE Proc. on Solid-State & Electron Devices–Part I*, Vol. 128, No. 5, pp. 180–184, 1981.

[14] H.C. Casey, M.B. Panish, "Heterosructure Lasers, part A and part B" *Academic Press*, 1978.

[15] L.A. Coldren, S.W. Corzine, "Diode Lasers and Photonic Integrated Circuits," *John Wiley & Sons, Inc.*, 1995.

[16] V. Rizzoli, A. Lipparini, A. Costanzo, F. Mastri, C. Cecchetti, A. Neri, D. Masotti, "State-of-the-art harmonic-balance simulation of forced nonlinear microwave circuits by the piecewise technique," *IEEE Transactions on Microwave Theory and Techniques*, Vol. 40, issue 1, pp. 12–28, Jan. 1992.

[17] S. N. Velu, *Charge Based Modeling in State Variable Based Simulator*, M.S. Thesis, Dept. of Electrical Engineering, North Carolina State University, 2002.

[18] W. I. Way, "Large Signal Nonlinear Distortion Prediction for a Single-Mode Laser Diode Under Microwave Intensity Modulation," *IEEE J. of Lightwave Technology*, Vol. LT-5, No. 3, March 1987.

[19] S. Iezekiel, C. M. Snowden, "Nonlinear Circuit Analysis of Laser Diodes Under Microwave Direct Modulation," *IEEE MTT-S International*, Vol. 2, pp. 937–940, 1990.

[20] E. Towe, R. F. Leheny, A. Yang, "A Historical Perspective of the Developement of the Vertical-Cavity Surface-Emitting Laser," *IEEE J. on Selected Topics in Quantum Electronics*, Vol.6, No. 6, Nov/Dec 2000.

[21] Y. Ohiso, K. Tateno, Y. Kohama, A. Wakatsuki, H. Tsunetsugu, and T. Kurokawa, "Flip-chip bonded 0.85-μm bottom-emitting vertical-cavity laser array on an AlGaAs substrate," *IEEE Photon. Technol. Lett.*, Vol. 8, pp. 1115-1117, Sep 1996.

[22] P. V. Mena, J. J. Morikuni, S.-M. Kang, A. V. Harton, K. W. Wyatt, "A Simple Rate-Equation-Based Thermal VCSEL Model," *IEEE J. of Lightwave Technology*, Vol. 17, No. 5, May 1999.

[23] M. A. Neifeld (private communication), 2003.

[24] G. Hasnain, K. Tai, L. Yang, Y. H. Wang, R. J. Fisher, J. D. Wynn, B. Weir, N. K. Dutta, and A. Y. Cho, "Performance of Gain-guided Surface Emitting Lasers with Semiconductor Distributed Bragg Reflectors," *IEEE J. of Quantum Electron.*, Vol. 27, No. 6, pp. 1377-1385, 1991.

[25] G. P. Agrawal, and N. K. Dutta, "Semiconductor Laser, 2nd ed." *New York: Van Nostrand Reinhold*, 1995.

[26] M. A. Neifeld and W. C. Chou, "Electrical packaging impact on source components in optical interconnect," *IEEE Transactions on Components, Packaging, and Manufacturing Technology — Part B*, Vol. 18, pp. 578–595, Aug. 1995.

[27] M. Bruensteiner, G. C. Papen, "Extraction of VCSEL Rate-Equation Parameters for Low-Bias System Simulation," *IEEE J. of Selected Topics in Quantum Electron*, Vol. 5, No. 3, 1999.

[28] C. Carlsson, H. Martinsson, R. Schatz, J. Halonen, A. Larsson "Analog Modulation Properties of Oxide Confined VCSELs at Microwave Frequencies," *IEEE J. of Lightwave Technology*, Vol. 20, No. 9, September 2002.

[29] A. F. Fernandez, F. Berghmans, B. Brichard, M. Decreton, "Toward The Developement of Radiation-Tolerant Instrumentation Data Links for Thermonuclear Fusion Experiments," *IEEE Transactin on Nuclear Science*, Vol. 49, No. 6, December 2002.

Version:
2003.01.01

Credits:

Name	Affiliation	Date	Logo
Houssam Kanj www.ncsu.edu	NC State University	2003	NC STATE UNIVERSITY